APPLIED SCIENCES AND ENGINEERING

Augmentation of brain tumor interstitial flow via focused ultrasound promotes brain-penetrating nanoparticle dispersion and transfection

Colleen T. Curley[1]*, Brian P. Mead[1]*, Karina Negron[2,3], Namho Kim[2,4], William J. Garrison[1], G. Wilson Miller[1,5], Kathryn M. Kingsmore[1], E. Andrew Thim[1], Ji Song[1], Jennifer M. Munson[6], Alexander L. Klibanov[1,7], Jung Soo Suk[2,3†], Justin Hanes[2,3,4†], Richard J. Price[1,5†]

Copyright © 2020 The Authors, some rights reserved; exclusive licensee American Association for the Advancement of Science. No claim to original U.S. Government Works. Distributed under a Creative Commons Attribution NonCommercial License 4.0 (CC BY-NC).

The delivery of systemically administered gene therapies to brain tumors is exceptionally difficult because of the blood-brain barrier (BBB) and blood-tumor barrier (BTB). In addition, the adhesive and nanoporous tumor extracellular matrix hinders therapeutic dispersion. We first developed the use of magnetic resonance image (MRI)–guided focused ultrasound (FUS) and microbubbles as a platform approach for transfecting brain tumors by targeting the delivery of systemically administered "brain-penetrating" nanoparticle (BPN) gene vectors across the BTB/BBB. Next, using an MRI-based transport analysis, we determined that after FUS-mediated BTB/BBB opening, mean interstitial flow velocity magnitude doubled, with "per voxel" flow directions changing by an average of ~70° to 80°. Last, we observed that FUS-mediated BTB/BBB opening increased the dispersion of directly injected BPNs through tumor tissue by >100%. We conclude that FUS-mediated BTB/BBB opening yields markedly augmented interstitial tumor flow that, in turn, plays a critical role in enhancing BPN transport through tumor tissue.

INTRODUCTION

Glioblastoma (GB) is the most common malignant primary brain tumor. Even with aggressive treatment, the median overall survival for patients with GB is only 15 months (*1*, *2*). Furthermore, brain metastases develop in roughly 10 to 20% of all patients with cancer (*3*). Promising new treatments for both primary and metastatic brain tumors, including gene therapy approaches, are constantly under development; however, brain neoplasms present tremendous challenges to effective therapeutic delivery. The delivery of systemically administered gene therapies to brain tumors is impeded by substantial physical barriers (*4*). First, while blood vessels within both primary and metastatic tumors may be leaky, this feature creates high interstitial fluid pressures that hinder convective transport of systemically administered gene therapies from the bloodstream and into the tissue (*5*, *6*). This is referred to as the blood-tumor barrier (BTB) (*5*). Second, when considering GB specifically, the blood-brain barrier (BBB) becomes a large obstacle to effective treatment because tumor cells invade surrounding healthy tissue where the BBB remains intact (*7*, *8*). Last, the transport of agents that have crossed into the brain tumor tissue compartment is limited by steric and adhesive interactions with the extracellular matrix (*9*).

Magnetic resonance image (MRI)–guided focused ultrasound (FUS) with circulating microbubbles (MBs) is a noninvasive approach for safe and reversible opening of the BTB and BBB. It is now well known that FUS application in the presence of intravascular MBs increases vascular permeability, which facilitates the delivery of systemically administered agents into brain tissue (*10*). Clinical trials using FUS and MBs for BTB/BBB opening for Alzheimer's disease and brain tumors (*11*, *12*) have been performed, with many others planned or underway. Preclinical work has established BTB/BBB opening with FUS and MBs as an effective method of delivery for antibodies, chemotherapies, and nanoparticles in both normal and diseased brain tissue (*10*, *13*–*19*). For gene delivery, FUS + MBs has been combined with both viral and nonviral gene vectors. Viral methods have mainly used adeno-associated virus (AAV) vectors, while nonviral methods include bubble conjugated liposomes, as well as targeted and nontargeted cationic bubble-plasmid conjugates (*20*–*26*). Our group has previously developed a nonviral gene delivery approach for transfection of brain tissue using FUS and polymeric "brain-penetrating" nanoparticle (BPN) gene vectors, an approach that may offer advantages over other methods (*13*, *14*, *27*, *28*). The first major component of this study entailed testing whether combining MRI–guided FUS + MB–mediated BTB/BBB opening with BPNs could elicit effective targeted brain tumor transfection.

The second major component of this investigation entailed determining how FUS + MB–mediated BTB/BBB opening affects both tumor interstitial fluid flow and BPN transport through tumor tissue. Because abnormal tumor vasculature contributes to high interstitial fluid pressure, pressure gradients across vessel walls are normally minimized, thereby limiting convective transport (*5*, *6*). However, recent evidence indicates that FUS + MB–mediated BTB/BBB opening could, in addition to augmenting the delivery of agents across the BTB/BBB, improve the penetration of therapeutics through both normal brain (*29*) and tumor tissue (*30*). To examine whether BTB/BBB opening with FUS and MBs affects interstitial transport in models of GB and brain metastases, we analyzed the spatiotemporal evolution of gadolinium transport via examination of a timed series of T1 contrast-enhanced MRIs (*31*). Next, after establishing how FUS + MB–mediated BTB/BBB opening affects interstitial transport,

[1]Department of Biomedical Engineering, University of Virginia, Charlottesville, VA 22908, USA. [2]Center for Nanomedicine at the Wilmer Eye Institute, Johns Hopkins University School of Medicine, Baltimore, MD 21231, USA. [3]Department of Pharmacology and Molecular Sciences, Johns Hopkins University School of Medicine, Baltimore, MD 21205, USA. [4]Department of Chemical and Biomolecular Engineering, Johns Hopkins University, Baltimore, MD 21218, USA. [5]Department of Radiology and Medical Imaging, University of Virginia, Charlottesville, VA 22908, USA. [6]Department of Biomedical Engineering and Mechanics, Virginia Polytechnic Institute and State University, Blacksburg, VA 24060, USA. [7]Cardiovascular Division, Department of Medicine, University of Virginia, Charlottesville, VA 22908, USA.
*These authors contributed equally to this work.
†Corresponding author. Email: rprice@virginia.edu (R.J.P.); hanes@jhmi.edu (J.H.); jsuk@jhmi.edu (J.S.S.)

we used a convection-enhanced delivery (CED) approach to assess the relative influence of BTB/BBB opening on BPN delivery versus its influence on BPN transport through tumor tissue. In summary, our results indicate that BTB/BBB opening with FUS and MBs does indeed facilitate brain tumor transfection with BPNs and provide evidence that a significant component of tumor transfection may be attributed to the augmented convective transport of BPNs through the interstitial space.

RESULTS

FUS and MBs facilitate the delivery of BPNs across the BTB/BBB

We first tested whether the activation of MBs with FUS could target the delivery of systemically administered BPNs to primary brain tumors under MRI guidance. Luciferase plasmid-bearing BPNs (Luc-BPNs) made with Cy5-labeled plasmid DNA (particle diameters of ~50 nm) was intravenously injected into athymic nude mice with intracranial U87 gliomas. The BTB/BBB was opened in and around tumors via MB activation with 1-MHz pulsed FUS [0.45- and 0.55-MPa peak negative pressure (PNP); measured in water], applied in an eight-spot grid. Acoustic emissions were assessed by passive cavitation detection during BTB/BBB opening. Roughly 6 hours following treatment, whole-brain and tumor samples from each animal were imaged for Cy5 fluorescence. Representative fluorescent images are shown in Fig. 1A (whole brain) and Fig. 1B (dissected tumor). For whole-brain images, fluorescence was measured using a region of interest (ROI) drawn to encompass the entire FUS-treated region, thus measuring delivery to the tumor and surrounding tissue. Quantification from whole-brain samples (Fig. 1C) showed that the Cy5 fluorescence signal was 3.5- and 4.5-fold higher in, respectively, 0.45- and 0.55-MPa FUS + MB–treated brains when compared to the BPN-only group. In tumor samples (Fig. 1D), Cy5 signal was 2.3-fold higher in the 0.55-MPa treatment group compared to the BPN-only group. The 0.45-MPa treatment group showed a trend toward an increase over the BPN-only group; however, this was not statistically significant ($P = 0.152$). Confocal microscopic observation of tumor cross sections confirmed that BPN delivery was augmented with FUS treatment and that BPNs penetrated well beyond tumor microvessels and into tissue (Fig. 1E). Acoustic emissions at the subharmonic (Fig. 1F), second harmonic (Fig. 1G), and third harmonic (Fig. 1H) were all significantly higher with 0.55-MPa FUS when compared to 0.45-MPa FUS. There were no differences in inertial cavitation at the two pressures (Fig. 1I).

BPN-mediated transgene expression is markedly enhanced in brain tumors treated with FUS and MBs

We next tested whether BPNs that had been delivered across the BTB/BBB with FUS and MBs was able to elicit significant tumor transgene expression. Luc-BPNs were intravenously injected immediately before FUS + MB BTB/BBB opening of U87mCherry and intracranial B16F1ova melanomas. Luciferase transgene expression was analyzed using ex vivo bioluminescence imaging of tumors 3 days after treatment. Representative ex vivo bioluminescence images of U87mCherry tumors are shown in Fig. 2A. In addition to the standard total flux bioluminescence measurement, average radiance was also quantified to ameliorate any possible influence of tumor size variability on transgene expression measurements. In both the U87mCherry and B16F1ova tumor models, FUS + MB BTB/BBB opening elicited significant, approximately fourfold, increases in both total flux and average radiance compared to mice receiving intravenous Luc-BPNs alone (Fig. 2, B to E). There were no differences in either total flux or average radiance between the 0.45- and 0.55-MPa PNP FUS groups.

Interstitial fluid transport in brain tumors is augmented by the application of FUS and MBs

For a subset of mice [$n = 4$ per group × 2 tumor types (U87mCherry and B16F1ova) × 2 PNPs (0.45 and 0.55 MPa) = 16 total], we used MRI to analyze the effect of BTB/BBB opening with FUS and MBs on gadolinium transport both to and within U87mCherry and B16F1ova intracranial tumors (*31*). To first assess BTB/BBB disruption following FUS + MB treatment, we calculated mean grayscale intensity from pre-FUS and post-FUS T1-weighted contrast-enhanced MRIs [Fig. 3A (U87) and Fig. 3D (B16F1ova)]. Tumors were visible in the pre-FUS images via gadolinium leakage from tumor vessels, which allowed MRI targeting of the treatment. Contrast enhancement was apparent in all post-FUS MRIs, indicating successful disruption of the BTB/BBB. As expected, mean grayscale intensity within tumors (i.e., ROI referred to as "BTB" and defined by enhancing region in pre-FUS image) significantly increased following FUS + MB treatment, as shown in Fig. 3B for U87 tumors and Fig. 3E for B16F1ova tumors. In addition, there was a significant increase in mean grayscale intensity in the entire FUS-treated region (i.e., ROI referred to as "BTB + BBB" and defined by enhancing region in the post-FUS image) in U87 and B16F1ova tumors (Fig. 3, C and F). Notably, opening the BTB/BBB with 0.55-MPa PNP FUS did not confer a detectable increase in contrast enhancement when compared to 0.45-MPa PNP FUS.

Pre- and post-FUS T1-weighted contrast-enhanced MRI sequences were then used to assess changes in interstitial fluid flow and diffusion. Representative MR imaging series in the U87mCherry tumor model are shown in Fig. 4A. These images were input into the post-processing algorithm, and an ROI in each animal was chosen to encompass the tumor and a portion of surrounding brain tissue. The algorithm solves for maps of flow velocity magnitude and direction, as well as diffusion coefficient. Figure 4B illustrates pre- and post-FUS flow velocity magnitude maps obtained from the imaging series. Flow velocities are plotted for each voxel within the selected ROI in Fig. 4C, showing a shift toward a higher velocity magnitude following FUS BTB/BBB opening in this tumor. Data from all animals showed a roughly twofold increase in mean flow velocity magnitude following BTB/BBB opening with FUS and MBs at both 0.45- and 0.55-MPa PNPs (Fig. 4D). Péclet number (Fig. 4E) changes mirrored interstitial flow velocity magnitude changes, indicating that diffusion coefficients were essentially unchanged with FUS + MB and that solute transport became even more convection dominant after FUS + MB. In U87mCherry tumors, intravoxel velocity direction changed by about 80°, on average, following BTB/BBB opening at both tested FUS pressures (Fig. 4, F to H). For the B16F1ova model, representative T1-weighted MRIs, flow velocity magnitude maps, and flow velocity voxel plots are shown in Fig. 5 (A, B, and C, respectively). We found a roughly twofold increase in mean flow velocity magnitude at both FUS pressures (Fig. 5D). Consistent with the U87 results, Péclet number changes (Fig. 5E) with FUS + MB mirrored interstitial flow velocity magnitude changes, while flow directions (Fig. 5, F to H) changed significantly. For U87 tumors, interstitial flow velocity changes elicited by FUS + MB did not correlate with tumor size, while a nonstatistically significant ($P = 0.1$) trend toward decreased interstitial flow with increasing tumor size was observed for B16F1ova tumors (fig. S1).

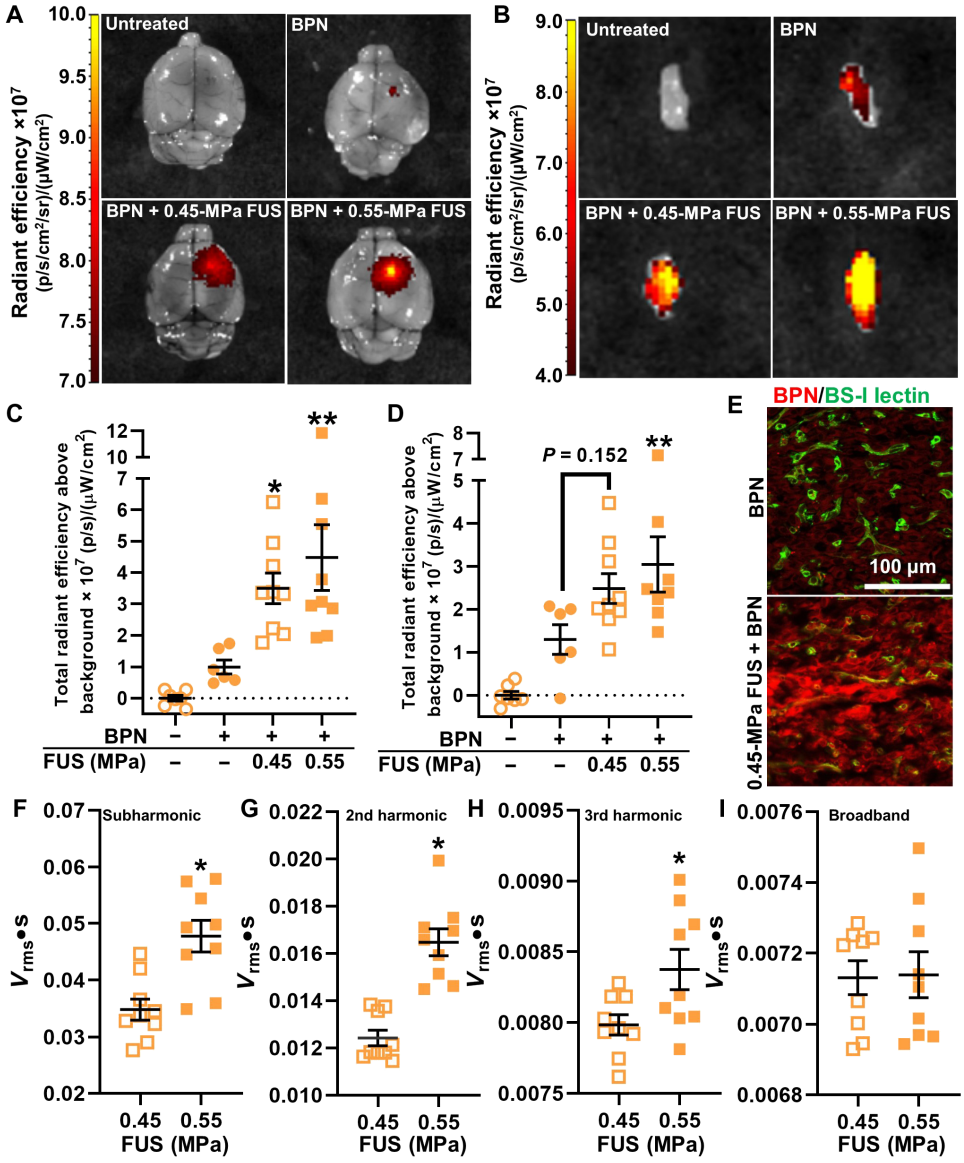

Fig. 1. MRI–guided delivery of intravenously administered BPNs to U87 gliomas and surrounding brain tissue with FUS. (**A**) Fluorescence images of whole brains with U87 tumors after treatment. p, photon. (**B**) Fluorescence images of excised U87 tumors after treatment. Tumors are ~2 to 3 mm in diameter. (**C**) Total fluorescence radiant efficiency in whole brains with U87 gliomas. Means ± SEM; $^*P = 0.047$ and $^{**}P = 0.0047$ versus BPN-only group, one-way analysis of variance (ANOVA) followed by Dunnett's multiple comparisons tests. (**D**) Total fluorescence radiant efficiency in excised U87 gliomas. Means ± SEM; $^{**}P = 0.026$ versus BPN-only group, one-way ANOVA followed by Dunnett's multiple comparisons tests. (**E**) Confocal images of BPNs (Cy5; red) with respect to tumor microvessels (BS-I lectin; green) showing penetration into tumor tissue. (**F** to **I**) Passive cavitation analyses for subharmonic ($^*P = 0.0014$) (F), second harmonic ($^*P < 0.0001$) (G), third harmonic ($^*P = 0.026$) (H), and inertial (not significant) (I) emissions. Unpaired *t* tests were used.

BTB opening with FUS and MBs augments BPN dispersion through brain tumors

Last, we tested whether modulation of interstitial flow with FUS and MBs during BTB/BBB opening could significantly affect BPN dispersion through brain tumor tissue. To this end, we performed FUS + MB–mediated BTB/BBB opening in intracranial U87mCherry tumors immediately before the CED of BPNs bearing the ZsGreen reporter gene (i.e., ZsGreen BPNs). Representative images showing ZsGreen transfection volume in the CED-only and FUS + MB BTB/BBB + CED groups are shown in Fig. 6A. We found a roughly two-fold enhancement in transfection volume in tumors treated with FUS + MB BTB/BBB opening before CED when compared to those receiving the CED injection only (Fig. 6B), indicating that FUS + MB–mediated BTB/BBB opening does indeed substantially augment BPN dispersion through tumor tissue.

DISCUSSION

The goals of this investigation were (i) to determine the efficacy of BTB/BBB opening with FUS and MBs as a means for targeted brain tumor transfection with systemically administered BPNs and (ii) to ascertain whether modulation of the physical tumor microenvironment

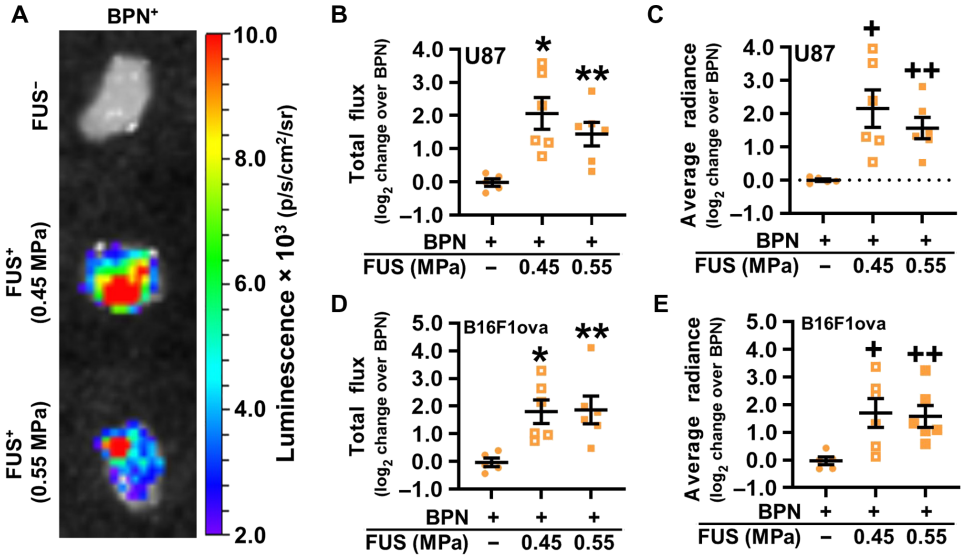

Fig. 2. MRI–guided transfection of brain tumors with intravenously administered BPNs and FUS. (**A**) Bioluminescence images of U87 tumors 3 days after treatment. Tumors are ~2 to 3 mm in diameter. (**B** and **C**) Luciferase expression in U87 gliomas, presented as total flux (B) and average radiance (C). Means ± SEM; *$P = 0.004$, **$P = 0.040$, +$P = 0.006$, and ++$P = 0.040$ versus BPN. (**D** and **E**) Luciferase expression in intracranial B16F1ova melanomas, presented as total flux (D) and average radiance (E). Means ± SEM; *$P = 0.020$, **$P = 0.016$, +$P = 0.027$, and ++$P = 0.040$ versus BPN. Significance was assessed in all graphs by one-way ANOVA followed by Tukey's *t* tests.

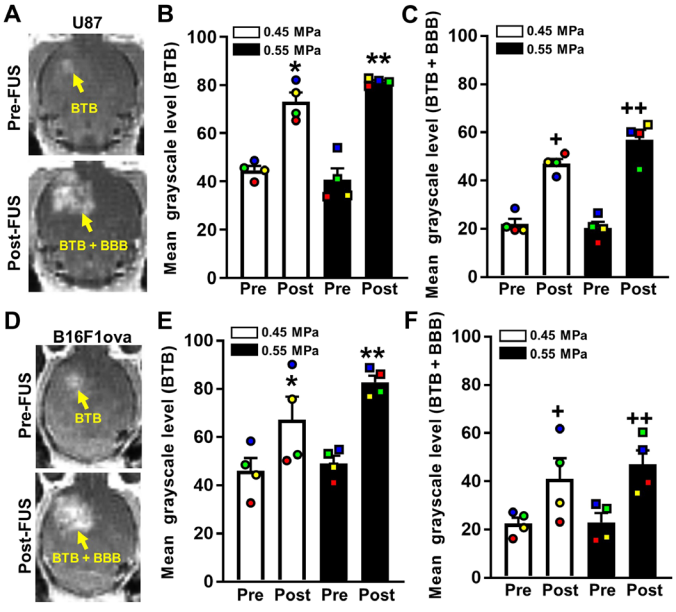

Fig. 3. BTB and BBB opening after application of MRI–guided FUS as assessed by T1-weighted contrast-enhanced MRI. (**A**) Pre- and post-FUS T1-weighted contrast MRIs of U87 gliomas. (**B** and **C**) Bar graphs of pre- and post-FUS mean grayscale levels in BTB (B) and BTB + BBB (C) ROIs, denoted by yellow arrows in (A). Paired data points are denoted by common colors and shapes. Bars, SEM. *$P = 0.0005$, **$P = 0.0001$, +$P = 0.003$, and ++$P = 0.0004$ versus "Pre" at same PNP. (**D**) Pre- and post-FUS T1-weighted contrast MRIs of B16F1ova melanomas. (**E** and **F**) Bar graphs of pre- and post-FUS mean grayscale levels in BTB (E) and BTB + BBB (F) ROIs. Bars, SEM. *$P = 0.017$, **$P = 0.0018$, +$P = 0.018$, and ++$P = 0.0053$ versus "Pre" at same PNP. Significance was assessed in all graphs by two-way repeated measures (RM) ANOVA followed by Sidak's multiple comparisons tests.

in conjunction with BTB/BBB opening promotes intratumor BPN transport. Under MRI guidance, BTB/BBB opening with FUS and MBs elicited a mean fourfold increase in U87 and B16F1ova brain tumor transfection over BPNs alone, with some tumors exhibiting as much as 16-fold increase in transfection. A T1 contrast-enhanced MRI-based analysis of gadolinium transport revealed that interstitial flow in brain tumors increased by an average of twofold after BTB/BBB opening, with most voxels also experiencing a marked shift (i.e., mean change of ~70° to 80°) in interstitial flow direction. BPNs that were injected directly into U87 tumors after BTB/BBB opening dispersed far more easily through tumor tissue (i.e., more than a doubling of transfection volume), providing strong evidence that modulation of the physical tumor microenvironment by FUS + MB–mediated BTB/BBB opening enhances BPN distribution throughout tumors after they have been delivered from the bloodstream. In all, this is the first study to demonstrate the successful MRI–guided transfection of both primary and metastatic brain tumors using nonviral brain-penetrating gene vectors in combination with FUS and MBs, as well as the first to use an MRI-based analysis to generate spatial maps of interstitial fluid flow changes in response to BTB/BBB opening with FUS and MBs. Our finding that augmented interstitial flow that plays a key role in dispersing a nonbioadhesive therapeutic through tumor tissue offers the enticing possibility that this insufficiently studied secondary effect of BTB/BBB opening with FUS and MBs can be leveraged to further improve therapeutic outcomes.

The BPNs used here are nonviral gene vectors designed to maximize distribution in brain tissue and thus offer many advantages over other gene carriers. Generally, polymeric nonviral gene vectors have an increased loading capacity, lower cost, and greater ability to tailor physiochemical properties than viral gene carriers. In addition, nonviral vectors alleviate concerns of preexisting immunity to naturally occurring viral vectors that could reduce efficacy and safety

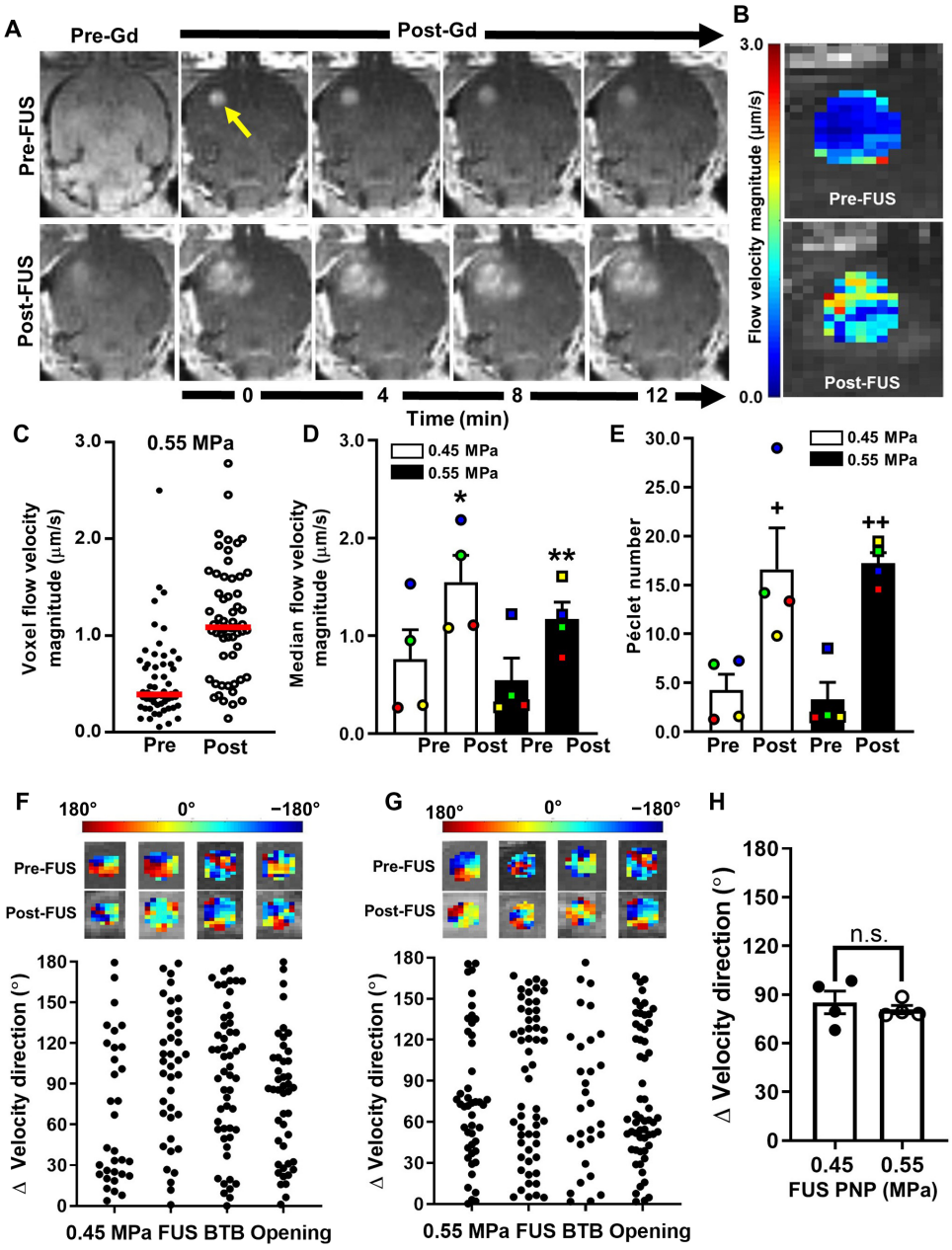

Fig. 4. BTB opening with MRI–guided FUS markedly alters interstitial flow velocity in U87 gliomas. (**A**) Pre- and post-FUS (0.55 MPa) T1-weighted contrast MRI sequences used for interstitial flow analyses. Arrow denotes enhancing tumor region used as the ROI for subsequent transport analysis. Gd, gadobenate dimeglumine contrast agent (MultiHance) administration. (**B**) Flow velocity magnitude map derived from the MRIs in (A). (**C**) Distribution of pre- and posttreatment voxel flow velocity magnitudes from (B). Red lines denote medians. (**D** and **E**) Plots of median flow velocity magnitudes (D) and Péclet numbers (E), pre- and posttreatment, with 0.45- and 0.55-MPa FUS. Paired data points are denoted by common colors and shapes. Bars, SEM. **P* = 0.01, ***P* = 0.04, +*P* = 0.01, and ++*P* = 0.005 versus "Pre" at same PNP. Significance was assessed by two-way RM ANOVA followed by Sidak's multiple comparisons tests. (**F** and **G**) Velocity direction changes in individual tumors due to BTB opening with 0.45-MPa (E) and 0.55-MPa (F) FUS. Each data point represents one voxel. (**H**) Mean velocity direction changes. Significance was tested by unpaired *t* test. n.s., not significant.

issues. Furthermore, the dense polyethylene glycol (PEG) coating on our brain-penetrating nonviral gene vectors facilitates increased spreading in brain tissue compared to conventionally PEGylated nanoparticles, resulting in enhanced vector distribution and transfection volume in both healthy brain and brain tumor tissues (*27*, *32*). Our group has previously demonstrated that FUS-mediated transfection of brain tissue with systemically administered BPNs occurs independent of overt signs of gliosis and off-target transfection (*13*, *14*, *28*). We have also proven therapeutic efficacy in a rat model of Parkinson's disease, in which we were able to achieve durable and therapeutic levels of glial cell line–derived neurotrophic factor transgene expression, thereby leading to restored dopamine levels and dopaminergic neuron content and reversed behavioral indicators of Parkinson's disease–associated motor dysfunction (*14*).

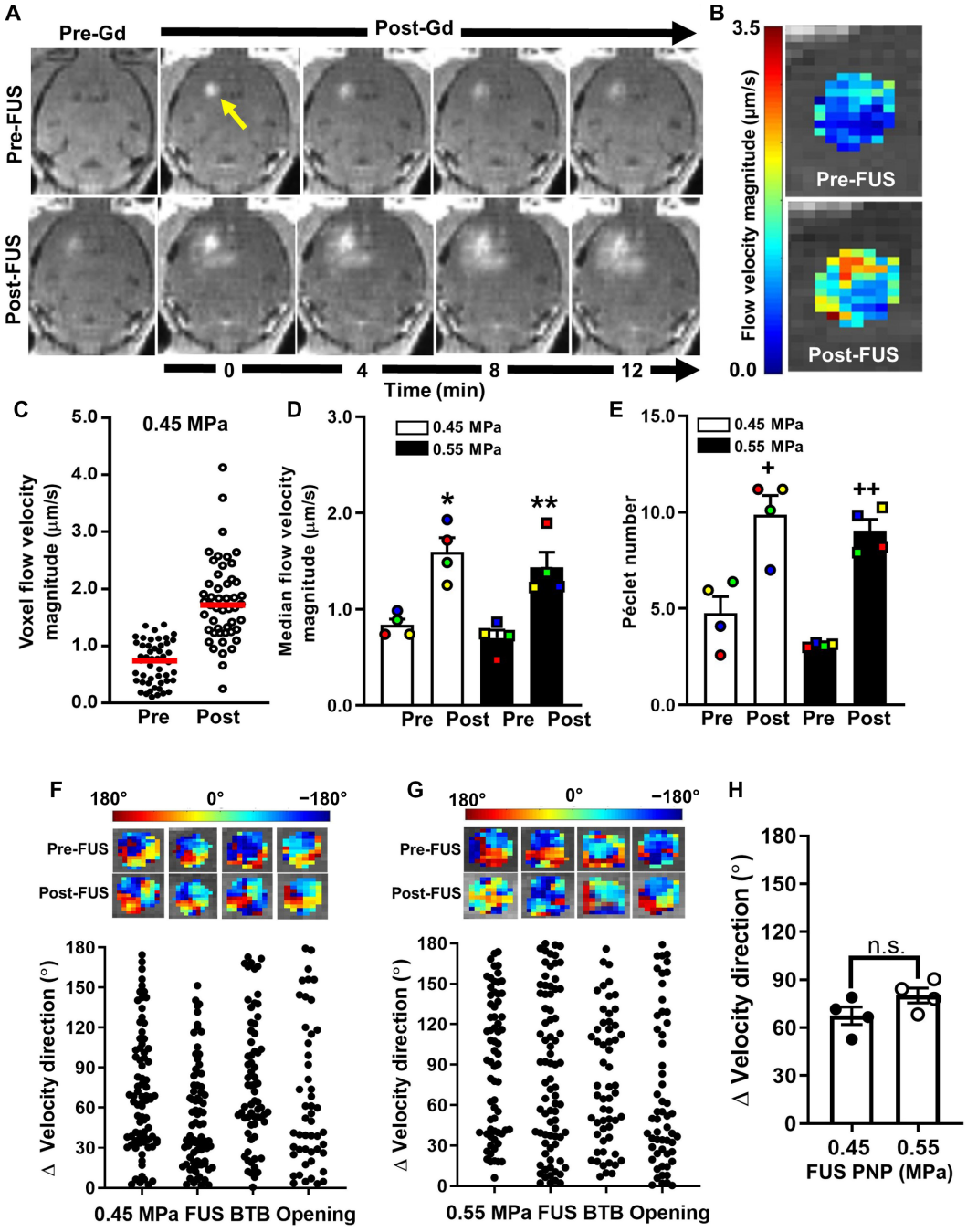

Fig. 5. BTB opening with MRI–guided FUS enhances interstitial fluid velocity in intracranial B16F1ova melanomas. (**A**) Representative pre- and post-FUS (0.45 MPa) T1-weighted contrast MRI sequences used for interstitial flow analyses. The arrow denotes enhancing tumor region used as the ROI for subsequent transport analysis. (**B**) Flow velocity magnitude map derived from the MRIs in (A). (**C**) Distribution of pre- and posttreatment voxel flow velocity magnitudes in (B). Red lines denote medians. (**D** and **E**) Plots of median flow velocity magnitudes (D) and Péclet numbers (E), pre- and posttreatment, with 0.45- and 0.55-MPa FUS. Paired data points are denoted by common colors and shapes. Bars, SEM. $*P = 0.014$, $**P = 0.016$, $+P = 0.004$, and $++P = 0.002$ versus "Pre" at same PNP. Significance was assessed by two-way RM ANOVA followed by Sidak's multiple comparisons tests. (**F** and **G**) Velocity direction changes in individual tumors due to BTB opening with 0.45-MPa (E) and 0.55-MPa (F) FUS. Each data point represents one voxel. (**H**) Mean velocity direction changes. Significance was tested by unpaired *t* test.

The use of FUS and BPNs to achieve gene expression in brain tumors described here represents a new strategy for brain tumor gene delivery that can overcome many of the challenges associated with more conventional methods. First, this approach is noninvasive, offering an advantage over direct injection methods for delivering gene vectors into brain tumor tissue. While some groups have achieved transfection of brain tumors following systemic administration of gene vectors, many rely upon the enhanced permeability and retention (EPR) effect for delivery into the tumor tissue. Use of the EPR effect alone can be ineffective because of the heterogeneous

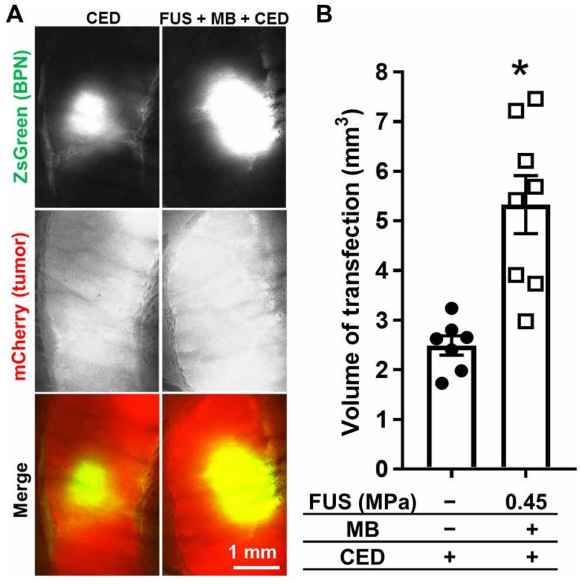

Fig. 6. BTB/BBB opening with FUS and MBs augments the penetration of BPNs through U87 gliomas. (**A**) Confocal images of ZsGreen transgene expression (green) in mCherry-expressing U87 gliomas (red). (**B**) Graph of ZsGreen transfection volumes. *$P = 0.0008$, unpaired *t* test.

vascular permeability and high interstitial fluid pressures that characterize the BTB (*5*, *6*). In addition, in GB, invasive cells infiltrate into normal brain tissue and reside behind the BBB. Thus, they cannot be reached by therapeutics delivered via the EPR effect (*8*). MB activation with FUS has the ability to transiently permeabilize vessels to overcome the BBB and BTB and allows for precise spatial targeting of the tumors and surrounding tissue where invasive cells reside. While the tumors used in this study are not invasive, we designed our treatment approach to target the entire tumor and the surrounding edges, which will be a crucial factor for therapeutic efficacy in invasive models of GB. On average, we achieved a fourfold increase in ex vivo bioluminescence in mice treated with FUS + MB BTB/BBB opening and Luc-BPNs compared to those receiving only an intravenous injection of Luc-BPNs. We saw similar efficacy in both the U87 and B16F1ova tumor models, representing primary and secondary brain tumors, respectively, suggesting that this approach is applicable across tumor models. That said, one limitation of our study was that we did not identify which cells within tumors were being transfected. Recently, we ascertained that both glioma cells and microglia are transfected after similarly formulated BPNs (*27*) are injected via CED. Thus, if necessary for a given application in the future, achieving cell specificity will likely require the use of targeting ligands and/or cell-specific promoters.

The lower PNP used in this study (0.45 MPa) was chosen on the basis of previous studies from our group (*13*, *14*), wherein we safely delivered similar-sized BPNs across the BBB in rats (160- to 200-g body weight) using the same albumin-shelled MB formulation and the same 1.1-MHz FUS system. In those studies, detailed histological examinations of brain tissue revealed no signs of damage when applying 0.6-MPa PNP FUS (measured in water). It is known that at frequencies in the range of 1.0 to 1.25 MHz, the middle region of the skull reduces FUS transmission no more than 20% for rats weighing between 160 and 200 g (*33*). This translates to an estimated nonderated PNP of 0.48 MPa in the rats. Thus, even if FUS attenuation by the skull in mice [measured to be 18% for 1.5-MHz FUS (*34*)] is not considered, the 0.45-MPa PNP used here is still below the safety threshold that we have previously established for these MBs in combination with this FUS system. If considering skull attenuation in mice, this PNP is well below the safety threshold.

From that baseline PNP of 0.45 MPa, we then chose to test whether increasing PNP could improve BPN delivery and transfection, as previous studies have shown enhanced size and volume of BBB opening with increasing PNP (*35*, *36*). A PNP of 0.55 MPa was chosen for this purpose because, while it enhances acoustic signatures associated with stable cavitation [i.e., subharmonic (Fig. 1E), second harmonic (Fig. 1F), and third harmonic (Fig. 1G)] in our system, it does not elicit a detectable increase in broadband signal associated with inertial cavitation (Fig. 1H), which could indicate the onset of microvascular and/or tissue damage (fig. 1H). Nonetheless, when considering BPN delivery (Fig. 1, A to D), tumor transfection (Fig. 2), BTB/BBB opening (Fig. 3), and interstitial fluid flow (Figs. 4 and 5), we unexpectedly observed no statistically significant differences between the two PNPs. Both of the tested pressures generate responses sufficient to (i) deliver ~50-nm-sized BPNs across the BTB/BBB and into the tissue and (ii) alter interstitial transport to promote BPN-mediated transfection (see forthcoming discussion). It is possible that, at least in the context of these specific experiments, our assays were insufficiently sensitive to detect differences between 0.45 and 0.55 MPa and/or that these differences in MB activation had no appreciable impact on key delivery metrics (Figs. 2 to 5). Further studies would be needed to determine the PNP below 0.45 MPa at which BPN delivery and transfection are compromised and whether further increasing PNP above 0.55 MPa yields improved delivery.

It is well established that activating MBs with FUS in the brain yields enhanced vascular permeability; however, there is now mounting evidence that modulation of the interstitial space is also an important factor facilitating agent delivery and distribution in targeted tissues. Very recent work using high-resolution imaging techniques coupled with physiologically based pharmacokinetic modeling demonstrated that FUS + MB BTB opening caused a shift from diffusion-dominated to convection-dominated transport in intracranial tumor tissue (*30*). Here, we explored how FUS + MB BTB opening alters the transport of agents in our intracranial tumor models and how this may aid in our ability to transfect brain tumor tissue with our nonviral gene vectors. Using an MRI-based technique to assess transport of gadolinium contrast agent, we measured a roughly twofold increase in flow velocity magnitude after FUS-mediated BTB/BBB opening, consistent with recent physiologically based pharmacokinetic model-derived results (*30*). While at least some of this increase in flow velocity magnitude is due to reduced hydraulic resistance of microvessel walls that separate higher pressure in the microvessel from lower pressure in the tumor tissue, it is also probable that FUS directly enhanced interstitial pore size and reduced tissue hydraulic resistance, an effect that has now been reported in multiple studies (*37*, *38*). Beyond increased fluid velocity magnitude, we also saw an ~70° to 80° change in interstitial flow direction. These changes could yield more frequent contact between BPNs and cells within the tumor, potentially allowing for enhanced uptake.

It has been shown previously that FUS + MB–induced increases in K_{trans}, a bulk measurement of gadobenate dimeglumine transport, are inversely correlated with tumor size in the rat 9L gliosarcoma model (*39*). To test whether similar relationships exist for interstitial

flow in the mouse U87 and B16F1ova models, we plotted changes in interstitial flow as a function of tumor size (fig. S1), as estimated by total voxels in the transport analysis. While not statistically significant in either mouse tumor model, consistent with rat 9L results (*39*), there was a trend ($P = 0.10$) toward decreased flow with increasing tumor size in the B16F1ova tumors. Given the potential significance of such a correlation, we submit that relationships between tumor size and FUS + MB–induced changes in interstitial flow warrant further study.

The MRI-based analysis provides us with a framework for understanding FUS-induced changes in transport of gadolinium in the tumor interstitial space; however, agent size and physiochemical properties play a significant role in determining transport dynamics. As diffusivity within a tissue is dependent, in part, on particle size, BPNs will have a smaller tissue diffusivity as compared to gadolinium chelates. Thus, with limited diffusivity, the movement of larger BPNs (~50 nm) through the tissue would be dominated by convection and sensitive to changes in interstitial flow velocity, a concept illustrated by the Péclet number. Conversely, the smaller gadolinium chelates (~0.75 nm) are likely to be transported via both diffusion and convection independent of the interstitial flow velocity magnitude. While it follows that spatiotemporal regions with lower calculated velocities may have a lower distribution of BPNs, testing this hypothesis would require assessing BPN delivery and transfection with more spatially precise approaches that allow for comparisons to interstitial flow maps.

The observation that gadolinium flow through tumor interstitial space is increased as a result of MB activation with FUS led us to experimentally test whether FUS + MB BTB/BBB opening also significantly alters transport of our larger (50 nm) BPN gene vectors. We found that FUS + MB–mediated BTB/BBB opening of intracranial U87mCherry xenograft tumors immediately before CED injection of BPNs resulted in a marked enhancement in transfection volume compared to CED injection alone. Notably, this result is consistent with previous studies wherein BBB opening with FUS and MBs enhanced the spread of AAV (*29*) and nonviral vectors (*28*) in normal brain tissue. While transfection volume in the FUS + MB + CED group (Fig. 6) could theoretically be affected by CED-injected BPNs that reenter the circulation and subsequently extravasate into tumor tissue downstream, we submit that this behavior would likely occur more readily in higher perfusion territories in the tumor. In turn, given the heterogeneous nature of tumor blood flow, this would yield oddly shaped distribution patterns with jagged edges, as opposed to the consistently uniform ellipsoidal distributions that we observed. Furthermore, given that the dispersion volume of CED-injected BPNs more than doubles after FUS + MB treatment, such an artifact would have to be profound to affect our results. The ability of FUS + MB–mediated BTB/BBB opening to promote the spread of BPNs supports the concept that enhanced interstitial fluid velocity facilitates the penetration of BPNs through tumor tissue, contributing to tumor transfection.

Last, we note that the MRI–targeted, noninvasive gene delivery approach described here represents a platform that can be combined with many other established and experimental approaches to generate innovative treatment strategies with the potential for superior efficacy. For example, immunotherapies hold much promise for long-lasting therapeutic responses in treatment of extracranial malignancies. The delivery of BPNs carrying immunomodulatory genes to brain tumors with FUS and MBs could be used to shift the balance from an immunosuppressive to an immunostimulatory tumor microenvironment to promote an antitumor immune response (*40*).

MATERIALS AND METHODS

Tumor implantation

Animal experiments were approved by the Animal Care and Use Committee at the University of Virginia and conformed to the National Institutes of Health guidelines for the use of animals in research. U87 glioma cells or U87 glioma cells that had been stably transfected with an mCherry reporter gene (i.e., U87mCherry) were implanted into 6- to 8-week-old male athymic nude mice purchased from Charles River Laboratories. B16F1ova melanoma cells were implanted in 8- to 10-week-old C57BL/6 mice, which were also purchased from Charles River Laboratories. Mice were anesthetized with a mixture of ketamine (40 mg/kg; Zoetis, Kalamazoo, MI) and Dexdomitor (0.2 mg/kg; Zoetis, Kalamazoo, MI) in 0.9% sterile saline and situated on a stereotaxic frame. Buprenorphine analgesic was subcutaneously administered. The surgical site was prepared with alternating scrubs of alcohol and iodine, and an incision was made at the midline of the scalp. A drill was used to create the burr hole located 2 mm to the right and 0.5 mm anterior to the bregma. A 10-μl Hamilton syringe with a 26-gauge needle was loaded with tumor cells (1.5×10^8 U87 cells/ml and 2.0×10^8 B16F1ova cells/ml). The needle tip was lowered to a depth of 4 mm below the skull surface and then withdrawn 1 mm to a final depth of 3 mm. A total volume of 2 μl of tumor cells (3×10^5 U87mCherry and U87 cells or 4×10^5 B16F1ova cells) were injected over 4 min. After one additional minute, the needle was slowly removed from the brain. The incision was closed with sutures and animals were given Antisedan to reverse the anesthesia.

BPN fabrication and characterization

BPNs were prepared as previously described (*27*). Briefly, methoxy-PEG-*N*-hydroxysuccinimide (5 kDa; Sigma-Aldrich, St. Louis, MO) was conjugated to 25-kDa branched polyethylenimine (PEI) (Sigma-Aldrich) to yield PEG-PEI copolymers, as previously described (*27*, *32*, *41*). Nuclear magnetic resonance (NMR) analysis was conducted to confirm PEG-to-PEI molar ratio of 50, a ratio previously shown to provide sufficient shielding of the BPN positive surface charge (*27*); 1H NMR (500 MHz, D_2O): δ 2.48 to 3.20 (br, CH_2CH_2NH), 3.62 to 3.72 (br, CH_2CH_2O). The green fluorescent reporter ZsGreen-expressing plasmids driven by the cytomegalovirus promoter was purchased from Clontech Laboratories Inc. (Mountain View, CA). The luciferase-expressing plasmid driven by human β-actin promoter (i.e., pBAL) was produced and provided by Copernicus Therapeutics (Cleveland, OH). The Mirus Label IT Tracker Intracellular Nucleic Acid Localization Kit (Mirus Bio, Madison, WI) was used to fluorescently tag plasmids with Cy5 fluorophores. BPNs were formed by dropwise addition of 10 volumes of labeled or unlabeled plasmids (0.2 mg/ml) to 1 volume of a swirling polymer solution at an optimized nitrogen-to-phosphate ratio of 6. BPN formulations were engineered by condensation of plasmids by a mixture of non-PEGylated PEI (25%) and PEG-PEI (75%). For IVIS imaging, Cy5-labeled plasmids were used to assemble fluorescently labeled BPNs. The plasmid/polymer solution was incubated for 30 min at room temperature to spontaneously form BPNs. Then, BPNs were washed twice with 3 volumes of ultrapure distilled water and reconcentrated to 1 mg/ml using Amicon Ultra Centrifugal Filters

(100,000 molecular weight cutoff; Millipore Corp., Billerica, MA). Plasmid concentration was determined via absorbance at 260 nm using a NanoDrop ND-1000 spectrophotometer (NanoDrop Technologies, Wilmington, DE). Last, the hydrodynamic diameters, polydispersity index, and ζ-potentials of BPNs were measured by dynamic light scattering and laser Doppler anemometry, respectively, in 10 mM NaCl solution at pH 7.0 using a Zetasizer Nano ZS90 (Malvern Instruments, Southborough, MA).

BTB/BBB opening with MRI–guided FUS and MBs

FUS treatments were applied 5 days after B16F1ova implantation and 7 days after U87mCherry or U87 implantation. Mice were anesthetized with a mixture of ketamine (40 mg/kg; Zoetis, Kalamazoo, MI) and Dexdomitor (0.2 mg/kg; Zoetis, Kalamazoo, MI) in 0.9% sterile saline, and tail veins were cannulated to allow for multiple intravenous injections. The MRI-guided FUS system (RK-100, FUS Instruments) sat directly on the patient table of a clinical 3-T MRI scanner (Siemens Prisma). Mice were placed supine on the MRI-guided FUS system with the skull sonically coupled to a 1.1-MHz spherically FUS transducer (with a 550-kHz hydrophone mounted in the center for passive cavitation detection) immersed in a degassed water bath. For the general treatment procedure, 0.05 ml of a MultiHance gadolinium contrast agent (105.8 mg/ml; Bracco Diagnostics) solution was administered intravenously, and a pre-FUS T1-weighted contrast-enhanced MRI of the entire brain was acquired using a custom-built 3-cm loop receive radio frequency coil and three-dimensional spoiled gradient echo pulse sequence. Pulse-sequence parameters for all T1-weighted images were identical: TR/TE, 12/4.35 ms; flip angle, 25°; readout bandwidth, 300 Hz/pixel; FOV (field of view), 38 by 77 by 36 mm; resolution, 0.3 mm isotropic; and total time per image. 3:04. Eight target spots were chosen from this presonication MRI to cover the entire tumor and surrounding tissue. To open the BTB/BBB, albumin-shelled MBs (1×10^5 per gram body weight; manufactured as previously described) (*42*) and Luc-BPNs (Luc-BPNs or Cy5-labeled Luc-BPNs; 1 μg/g body weight) were intravenously injected, and FUS was applied to the targets using 0.45- or 0.55-MPa PNP (measured in water). FUS was applied in 10-ms pulses with a 2-s pulsing interval (i.e., 0.5% duty cycle) for a total of 2 min. Animals were then reinjected with gadolinium contrast agent and postsonication T1-weighted contrast-enhanced MRIs were acquired to confirm BTB/BBB opening. Following treatment, mice were given Antisedan to reverse the anesthesia. In a subset of the Luc-BPN delivery cohort ($n = 4$ per group × 2 tumor types × 2 PNPs = 16 total, referred to as "TM" for transport mice), this general procedure was varied to include additional MR imaging for transport analysis as described below.

MR imaging for transport analysis

TM were imaged with MRI using an alternative protocol to permit interstitial tumor transport analysis. For these animals, a three-dimensional T1-weighted MRI was acquired immediately before the injection of the contrast agent to obtain the baseline signal intensity in the tissue. The contrast agent was then intravenously injected, and a series of four T1-weighted contrast-enhanced MRIS were obtained. Pulse-sequence parameters for all T1-weighted Is were identical: TR/TE, 12/4.35 ms; flip angle, 25°; readout bandwidth, 300 Hz/Px; FOV, 38 by 77 by 36 mm; resolution, 0.3 mm isotropic; and total time per image, 3:04. Following FUS BTB/BBB opening (described previously), a T1-weighted MRI was again acquired to obtain baseline signal intensity for post-FUS measurements. The contrast agent was injected intravenously, and a second series of four T1-weighted contrast-enhanced MRIs was acquired.

MRI analysis for grayscale intensity

For TM, the first T1-weighted MRI in the pre- and post-FUS contrast-enhanced imaging series was analyzed for grayscale intensity of gadolinium enhancement. Two different ROIs were analyzed, one encompassing the entire FUS-targeted region, referred to as "BTB + BBB," and one encompassing only the tumor, referred to as "BTB." Mean pixel grayscale intensity was quantified within each of these ROIs in the pre-FUS and post-FUS images for each animal. An equivalent ROI was chosen on the contralateral side, and the grayscale intensity was subtracted as background.

Transport analysis

We analyzed the spatiotemporal evolution of gadolinium transport in tumors using a recently described approach (*31*). Briefly, for each pre-FUS and post-FUS imaging series, the acquired images were loaded into the postprocessing algorithm. The precontrast image was subtracted from the postcontrast series to remove background signal. For each animal, the ROI was chosen to encompass the entire enhancing region from the pre-FUS images and a portion of surrounding non-enhancing tissue, and the same ROI was used to analyze pre- and post-FUS sequences. The tissue slice analyzed in the algorithm corresponded to the coordinate that was targeted for FUS BTB/BBB opening. The spatiotemporal evolution of solute concentration, in this case, gadolinium, can be approximated by a differential equation dependent on input velocity and diffusion coefficient. Using the gadolinium signal intensity over time acquired in the T1-weighted MRIs, the algorithm solves the inverse problem to estimate diffusion coefficients and interstitial fluid velocities within the selected ROI.

The model uses a forward-time, centered-in-space method. Because of the diffusion term, it is unconditionally numerically stable. The partial differential equation is solved for one time step at a time, and this solution is used to compute an approximation for the inverse problem. Thus, errors do not accumulate over time steps. While the model has not been compared to direct in vivo transport measurements, it has been carefully validated using flow phantoms in vitro (*31*).

Using this technique, we obtained spatial maps of fluid velocity magnitude and direction and diffusion coefficient for the selected ROI before and after FUS + MB BTB/BBB opening. Péclet number was calculated per voxel as $v \times L/D$, where v is the velocity, L is the characteristic length (voxel dimension), and D is the diffusion coefficient. In some tumors, a fraction of voxels had insufficient image contrast, causing the model to return a null diffusion coefficient. These voxels were disregarded in the Péclet number calculations.

Passive cavitation detection

Acoustic emissions were detected with a 2.5-mm wideband unfocused hydrophone mounted in the center of the transducer. Acoustic signal was captured using a scope card (ATS460, Alazar, Pointe-Claire, Canada) and processed using an in-house-built MATLAB algorithm. Acoustic emissions at the fundamental frequency, harmonics (2f, 3f, and 4f), subharmonic (0.5f), and ultraharmonics (1.5f, 2.5f, and 3.5f) were assessed by first taking the root mean square of the peak spectral amplitude (V_{rms}) in each frequency band after applying a 5-kHz bandwidth filter and then summing the product of V_{rms} and

individual sonication duration over the entire treatment period. Inertial cavitation was assessed by summing the product of V_{rms} and individual sonication duration for all remaining emissions (broadband) over the entire treatment period.

Ex vivo fluorescence imaging

Roughly 6 hours following BTB/BBB with FUS and MBs for delivery of Cy5-labeled Luc-BPN delivery to U87 tumors, mice were euthanized via intraperitoneal injection of Euthasol. Brains were removed and imaged on the IVIS Spectrum for Cy5 fluorescence signal using the 640/680 excitation/emission filter set and auto exposure settings. Tumors were then immediately removed and imaged using the same settings. For whole-brain images, an identical circular ROI was used for every sample. For tumor images, the ROIs were drawn around the tumor edges for each sample to encompass the entire tumor. Cy5 fluorescence was quantified for both whole-brain and tumor samples using described ROIs and reported as radiant efficiency.

Ex vivo bioluminescence imaging

Three days following BTB/BBB with FUS and MBs for Luc-BPN delivery, mice were given an intraperitoneal injection of D-luciferin (Gold Biotechnology, St. Louis, MO) at a dose of 150 mg/kg. Five minutes later, mice were euthanized via intraperitoneal injection of Euthasol, and the tumor tissue was harvested. Tumors were incubated in a solution of D-luciferin (1 mg/ml) for 3 min, and bioluminescence imaging was performed on the IVIS Spectrum using a 3-min exposure time. Using the Living Image software, ROIs were drawn around the tumor edges to encompass the entire tumor sample. Photon flux was quantified and reported as total flux and average radiance.

CED of ZsGreen BPNs after BTB/BBB opening with FUS and MBs

U87mCherry tumor cells were implanted 16 days before treatment, as previously described. The day 16 time point was chosen so that the tumors would be easier to target with our CED injections. Mice were anesthetized with a mixture of ketamine (40 mg/kg; Zoetis, Kalamazoo, MI) and Dexdomitor (0.2 mg/kg; Zoetis, Kalamazoo, MI) in 0.9% sterile saline. Buprenorphine analgesic was administered subcutaneously. Tail veins were cannulated in a subset of mice to facilitate intravenous injection of MBs, and mice were situated in a stereotaxic frame (Stoelting, Wood Dale, IL). For mice receiving FUS + MB BTB/BBB opening, heads were ultrasonically coupled to a 1-MHz single-element FUS transducer (Olympus, Center Valley, NJ) with degassed ultrasound gel. The transducer was positioned so that the focus coincided with the location of the tumor in the right striatum. Albumin-shelled MBs were intravenously injected (1×10^5 MBs/g), and FUS was applied at a 0.45-MPa PNP with a 0.5% duty cycle (10 ms, every 2 s, for 2 min). Note that this BTB/BBB opening protocol is identical to that used to deliver Luc-BPNs under MRI guidance. Immediately following sonication, the CED procedure commenced. To prepare for CED, heads were cleaned with alternating wipes of alcohol and iodine. A midline scalp incision was made to expose the skull, and a drill was used to create a burr hole at the appropriate location to target the tumor. A Neuros syringe (Neuros 1705, Hamilton, Reno, NV) containing a 33-gauge needle and a 1-mm step was inserted at 1 mm/min to the appropriate depth (coordinates determined from T1-weighted MRIs acquired 1 day before CED injections). The infusion rate was set to 0.33 μl/min using a frame-mounted syringe pump (UMP3, World Precision Instruments, Sarasota, USA). A total of 19 μg of ZsGreen-BPNs in 20 μl of 0.9% NaCl was injected. Five minutes following the completion of the injection, the needle was slowly removed at 1 mm/min and the burr hole was filled with sterile bone wax.

Confocal imaging and quantification of ZsGreen transfection volume

Approximately 48 hours following CED of ZsGreen BPNs, mice were euthanized and transcardially perfused with 10 ml of 2% heparinized 0.9% saline, followed by 10 ml of tris-buffered saline with calcium chloride (0.1 g/liter). Brains were removed, rapidly frozen to −80°C, and cut into 100-μm sections using a cryostat (1905, Leica, Buffalo Grove, IL). Every other section within 2 to 3 mm of the injection site was collected on a slide and mounted with permanent mounting medium (P36970, Invitrogen, Carlsbad, USA). Sections were imaged using a Nikon Eclipse TE2000 confocal microscope (Nikon, Melville, NY) under ×4 magnification. Multiple images were taken and stitched together in montages to capture the entire injection site. Volume of transfected tumor tissue was quantified from these images using a MATLAB script similar to previous studies (*32*). Briefly, background fluorescence was subtracted and images were thresholded at 5% of the maximum intensity. The total volume of transgene expression was calculated by multiplying the area of distribution from each slice by the slice thickness and summing values for each slice.

Statistical analysis

A detailed description of statistical methods for each experiment is provided in the corresponding figure legend. "*n*" values per group are evident in all figure panels with statistical comparisons, as all individual data points are represented.

SUPPLEMENTARY MATERIAL

Supplementary material for this article is available at http://advances.sciencemag.org/cgi/content/full/6/18/eaay1344/DC1

View/request a protocol for this paper from *Bio-protocol*.

REFERENCES AND NOTES

1. Q. T. Ostrom, H. Gittleman, P. Liao, C. Rouse, Y. Chen, J. Dowling, Y. Wolinsky, C. Kruchko, J. Barnholtz-Sloan, CBTRUS statistical report: Primary brain and central nervous system tumors diagnosed in the united states in 2007-2011. *Neuro Oncol.* **16**, iv1–iv63 (2014).
2. R. Stupp, W. P. Mason, M. J. van den Bent, M. Weller, B. Fisher, M. J. B. Taphoorn, K. Belanger, A. A. Brandes, C. Marosi, U. Bogdahn, J. Curschmann, R. C. Janzer, S. K. Ludwin, T. Gorlia, A. Allgeier, D. Lacombe, J. G. Cairncross, E. Eisenhauer, R. Mirimanoff; European Organisation for Research and Treatment of Cancer Brain Tumor and Radiotheraphy Groups; National Cancer Institute of Canada Clinical Trials Group, Radiotherapy plus concomitant and adjuvant temozolomide for glioblastoma. *N. Engl. J. Med.* **352**, 987–996 (2005).
3. H. Takei, E. Rouah, Y. Ishida, Brain metastasis: Clinical characteristics, pathological findings and molecular subtyping for therapeutic implications. *Brain Tumor Pathol.* **33**, 1–12 (2016).
4. G. F. Woodworth, G. P. Dunn, E. A. Nance, J. Hanes, H. Brem, Emerging insights into barriers to effective brain tumor therapeutics. *Front. Oncol.* **4**, 126 (2014).
5. O. van Tellingen, B. Yetkin-Arik, M. C. de Gooijer, P. Wesseling, T. Wurdinger, H. E. de Vries, Overcoming the blood–brain tumor barrier for effective glioblastoma treatment. *Drug Resist. Updat.* **19**, 1–12 (2015).
6. R. K. Jain, T. Stylianopoulos, Delivering nanormedicine to solid tumors. *Nat. Rev. Clin. Oncol.* **7**, 653–664 (2010).
7. W. M. Pardridge, The blood-brain barrier: Bottleneck in brain drug development. *NeuroRx* **2**, 3–14 (2005).

8. R. K. Oberoi, K. E. Parrish, T. T. Sio, R. K. Mittapalli, W. F. Elmquist, J. N. Sarkaria, Strategies to improve delivery of anticancer drugs across the blood-brain barrier to treat glioblastoma. *Neuro Oncol.* **18**, 27–36 (2015).
9. E. Syková, C. Nicholson, Diffusion in brain extracellular space. *Physiol. Rev.* **88**, 1277–1340 (2008).
10. K. F. Timbie, B. P. Mead, R. J. Price, Drug and gene delivery across the blood-brain barrier with focused ultrasound. *J. Control. Release* **219**, 61–75 (2015).
11. N. Lipsman, Y. Meng, A. J. Bethune, Y. Huang, B. Lam, M. Masellis, N. Herrmann, C. Heyn, I. Aubert, A. Boutet, G. S. Smith, K. Hynynen, S. E. Black, Blood-brain barrier opening in Alzheimer's disease using MR-guided focused ultrasound. *Nat. Commun.* **9**, 2336 (2018).
12. T. Mainprize, N. Lipsman, Y. Huang, Y. Meng, A. Bethune, S. Ironside, C. Heyn, R. Alkins, M. Trudeau, A. Sahgal, J. Perry, K. Hynynen, Blood-brain barrier opening in primary brain tumors with non-invasive MR-guided focused ultrasound: A clinical safety and feasibility study. *Sci. Rep.* **9**, 321 (2019).
13. B. P. Mead, P. Mastorakos, J. S. Suk, A. L. Klibanov, J. Hanes, R. J. Price, Targeted gene transfer to the brain via the delivery of brain-penetrating DNA nanoparticles with focused ultrasound. *J. Control. Release* **223**, 109–117 (2016).
14. B. P. Mead, N. Kim, G. W. Miller, D. Hodges, P. Mastorakos, A. L. Klibanov, J. W. Mandell, J. Hirsh, J. S. Suk, J. Hanes, R. J. Price, Novel focused ultrasound gene therapy approach noninvasively restores dopaminergic neuron function in a rat Parkinson's disease model. *Nano Lett.* **17**, 3533–3542 (2017).
15. E. Nance, K. Timbie, G. W. Miller, J. Song, C. Louttit, A. L. Klibanov, T. Y. Shih, G. Swaminathan, R. J. Tamargo, G. F. Woodworth, J. Hanes, R. J. Price, Non-invasive delivery of stealth, brain-penetrating nanoparticles across the blood–brain barrier using MRI-guided focused ultrasound. *J. Control. Release* **189**, 123–132 (2014).
16. K. F. Timbie, U. Afzal, A. Date, C. Zhang, J. Song, G. Wilson Miller, J. S. Suk, J. Hanes, R. J. Price, MR image-guided delivery of cisplatin-loaded brain-penetrating nanoparticles to invasive glioma with focused ultrasound. *J. Control. Release* **263**, 120–131 (2017).
17. L. H. Treat, N. McDannold, Y. Zhang, N. Vykhodtseva, K. Hynynen, Improved anti-tumor effect of liposomal doxorubicin after targeted blood-brain barrier disruption by MRI-guided focused ultrasound in rat glioma. *Ultrasound Med. Biol.* **38**, 1716–1725 (2012).
18. E.-J. Park, Y.-Z. Zhang, N. Vykhodtseva, N. McDannold, Ultrasound-mediated blood-brain/blood-tumor barrier disruption improves outcomes with trastuzumab in a breast cancer brain metastasis model. *J. Control. Release* **163**, 277–284 (2012).
19. M. Kinoshita, N. McDannold, F. A. Jolesz, K. Hynynen, Noninvasive localized delivery of herceptin to the mouse brain by MRI-guided focused ultrasound-induced blood-brain barrier disruption. *Proc. Natl. Acad. Sci. U.S.A.* **103**, 11719–11723 (2006).
20. S. Wang, O. O. Olumolade, T. Sun, G. Samiotaki, E. E. Konofagou, Noninvasive, neuron-specific gene therapy can be facilitated by focused ultrasound and recombinant adeno-associated virus. *Gene Ther.* **22**, 104–110 (2015).
21. K. Xhima, F. Nabbouh, K. Hynynen, I. Aubert, A. Tandon, Noninvasive delivery of an α-synuclein gene silencing vector with magnetic resonance-guided focused ultrasound. *Mov. Disord.* **33**, 1567–1579 (2018).
22. C. H. Fan, E. L. Chang, C. Y. Ting, Y. C. Lin, E. C. Liao, C. Y. Huang, Y. C. Chang, H. L. Chan, K. C. Wei, C. K. Yeh, Folate-conjugated gene-carrying microbubbles with focused ultrasound for concurrent blood-brain barrier opening and local gene delivery. *Biomaterials* **106**, 46–57 (2016).
23. C. Y. Lin, H. Y. Hsieh, W. G. Pitt, C. Y. Huang, I. C. Tseng, C. K. Yeh, K. C. Wei, H. L. Liu, Focused ultrasound-induced blood-brain barrier opening for non-viral, non-invasive, and targeted gene delivery. *J. Control. Release* **212**, 1–9 (2015).
24. E. L. Chang, C. Y. Ting, P. H. Hsu, Y. C. Lin, E. C. Liao, C. Y. Huang, Y. C. Chang, H. L. Chan, C. S. Chiang, H. L. Liu, K. C. Wei, C. H. Fan, C. K. Yeh, Angiogenesis-targeting microbubbles combined with ultrasound-mediated gene therapy in brain tumors. *J. Control. Release* **255**, 164–175 (2017).
25. G. Zhao, Q. Huang, F. Wang, X. Zhang, J. Hu, Y. Tan, N. Huang, Z. Wang, Z. Wang, Y. Cheng, Targeted shRNA-loaded liposome complex combined with focused ultrasound for blood brain barrier disruption and suppressing glioma growth. *Cancer Lett.* **418**, 147–158 (2018).
26. P. Yue, W. Miao, L. Gao, X. Zhao, J. Teng, Ultrasound-triggered effects of the microbubbles coupled to GDNF plasmid-loaded PEGylated liposomes in a rat model of Parkinson's disease. *Front. Neurosci.* **12**, 222 (2018).
27. K. Negron, N. Khalasawi, B. Lu, C. Y. Ho, J. Lee, S. Shenoy, H. Q. Mao, T. H. Wang, J. Hanes, J. S. Suk, Widespread gene transfer to malignant gliomas with in vitro-to-in vivo correlation. *J. Control. Release* **303**, 1–11 (2019).
28. B. P. Mead, C. T. Curley, N. Kim, K. Negron, W. J. Garrison, J. Song, D. Rao, G. W. Miller, J. W. Mandell, B. W. Purow, J. S. Suk, J. Hanes, R. J. Price, Focused ultrasound preconditioning for augmented nanoparticle penetration and efficacy in the central nervous system. *Small* **15**, e1903460 (2019).
29. S. Wang, M. E. Karakatsani, C. Fung, T. Sun, C. Acosta, E. Konofagou, Direct brain infusion can be enhanced with focused ultrasound and microbubbles. *J. Cereb. Blood Flow Metab.* **37**, 706–714 (2016).
30. C. D. Arvanitis, V. Askoxylakis, Y. Guo, M. Datta, J. Kloepper, G. B. Ferraro, M. O. Bernabeu, D. Fukumura, N. McDannold, R. K. Jain, Mechanisms of enhanced drug delivery in brain metastases with focused ultrasound-induced blood-tumor barrier disruption. *Proc. Natl. Acad. Sci. U.S.A.* **115**, E8717–E8726 (2018).
31. K. M. Kingsmore, A. Vaccari, D. Abler, S. X. Cui, F. H. Epstein, R. C. Rockne, S. T. Acton, J. M. Munson, MRI analysis to map interstitial flow in the brain tumor microenvironment. *APL Bioeng.* **2**, 031905 (2018).
32. P. Mastorakos, C. Zhang, S. Berry, Y. Oh, S. Lee, C. G. Eberhart, G. F. Woodworth, J. S. Suk, J. Hanes, Highly PEGylated DNA nanoparticles provide uniform and widespread gene transfer in the brain. *Adv. Healthc. Mater.* **4**, 1023–1033 (2015).
33. M. Gerstenmayer, B. Fellah, R. Magnin, E. Selingue, B. Larrat, Acoustic transmission factor through the rat skull as a function of body mass, frequency and position. *Ultrasound Med. Biol.* **44**, 2336–2344 (2018).
34. J. J. Choi, M. Pernot, S. A. Small, E. E. Konofagou, Noninvasive, transcranial and localized opening of the blood-brain barrier using focused ultrasound in mice. *Ultrasound Med. Biol.* **33**, 95–104 (2007).
35. Y.-S. Tung, F. Vlachos, J. A. Feshitan, M. A. Borden, E. E. Konofagou, The mechanism of interaction between focused ultrasound and microbubbles in blood-brain barrier opening in mice. *J. Acoust. Soc. Am.* **130**, 3059–3067 (2011).
36. H. Chen, E. E. Konofagou, The size of blood–brain barrier opening induced by focused ultrasound is dictated by the acoustic pressure. *J. Cereb. Blood Flow Metab.* **34**, 1197–1204 (2014).
37. D. S. Hersh, B. A. Nguyen, J. G. Dancy, A. R. Adapa, J. A. Winkles, G. F. Woodworth, A. J. Kim, V. Frenkel, Pulsed ultrasound expands the extracellular and perivascular spaces of the brain. *Brain Res.* **1646**, 543–550 (2016).
38. D. S. Hersh, P. Anastasiadis, A. Mohammadabadi, B. A. Nguyen, S. Guo, J. A. Winkles, A. J. Kim, R. Gullapalli, A. Keller, V. Frenkel, G. F. Woodworth, MR-guided transcranial focused ultrasound safely enhances interstitial dispersion of large polymeric nanoparticles in the living brain. *PLOS ONE* **13**, e0192240 (2018).
39. M. Aryal, J. Park, N. Vykhodtseva, Y.-Z. Zhang, N. McDannold, Enhancement in blood-tumor barrier permeability and delivery of liposomal doxorubicin using focused ultrasound and microbubbles: Evaluation during tumor progression in a rat glioma model. *Phys. Med. Biol.* **60**, 2511–2527 (2015).
40. C. T. Curley, N. D. Sheybani, T. N. Bullock, R. J. Price, Focused ultrasound immunotherapy for central nervous system pathologies: Challenges and opportunities. *Theranostics* **7**, 3608–3623 (2017).
41. J. S. Suk, A. J. Kim, K. Trehan, C. S. Schneider, L. Cebotaru, O. M. Woodward, N. J. Boylan, M. P. Boyle, S. K. Lai, W. B. Guggino, J. Hanes, Lung gene therapy with highly compacted DNA nanoparticles that overcome the mucus barrier. *J. Control. Release* **178**, 8–17 (2014).
42. C. W. Burke, J. S. Suk, A. J. Kim, Y. H. J. Hsiang, A. L. Klibanov, J. Hanes, R. J. Price, Markedly enhanced skeletal muscle transfection achieved by the ultrasound-targeted delivery of non-viral gene nanocarriers with microbubbles. *J. Control. Release* **162**, 414–421 (2012).

Acknowledgments: We thank R. Abounader for providing U87 cells and R. C. Rockne and D. Abler for insight into the mathematical basis of the transport model. **Funding:** R.J.P., J.H., and J.S.S. were supported by NIH R01CA164789, R01CA197111, R01CA204968, and R01EB020147. J.M.M. was supported by NIH R372222563. A.L.K. was supported by NIH R01EB023055. K.M.K. was supported by an NSFGRF. **Author contributions:** C.T.C., J.S., and B.P.M. performed experimental work. C.T.C., B.P.M., and R.J.P. analyzed the data. C.T.C., B.P.M., and R.J.P. conceived the experiments, with input from J.S.S., K.M.K., and J.M.M. K.N., N.K., J.S.S., and J.H. provided BPNs. A.L.K. provided MBs. G.W.M. and W.J.G. developed MRI sequences and performed MR imaging. K.M.K. and J.M.M. contributed to the conception and execution of the MRI-based transport analysis. E.A.T. performed the analysis of cavitation data. C.T.C. and R.J.P. wrote the manuscript. **Competing interests:** The authors declare that they have no competing interests. **Data and materials availability:** All data needed to evaluate the conclusions in the paper are present in the paper and/or the Supplementary Materials. Additional data related to this paper may be requested from the authors.

Submitted 27 May 2019
Accepted 11 February 2020
Published 1 May 2020
10.1126/sciadv.aay1344

Citation: C. T. Curley, B. P. Mead, K. Negron, N. Kim, W. J. Garrison, G. W. Miller, K. M. Kingsmore, E. A. Thim, J. Song, J. M. Munson, A. L. Klibanov, J. S. Suk, J. Hanes, R. J. Price, Augmentation of brain tumor interstitial flow via focused ultrasound promotes brain-penetrating nanoparticle dispersion and transfection. *Sci. Adv.* **6**, eaay1344 (2020).